RSC Advances

PAPER

View Article Online
View Journal | View Issue

Cite this: *RSC Adv.*, 2017, **7**, 51593

Mussel-inspired deposition of copper on titanium for bacterial inhibition and enhanced osseointegration in a periprosthetic infection model

Lei Wang,†[a] Xing Yang,†[a] Weiwei Cao,[b] Chen Shi,[c] Pinghui Zhou,[a] Qiang Li,[b] Fengxuan Han,[a] Junying Sun,*[a] Xiaodong Xing*[b] and Bin Li *[ad]

Periprosthetic infection represents one of the most devastating complications in orthopedic surgeries. Implants that have both anti-bacterial and bone-forming capability and may function to simultaneously clear infection and repair bone defect, therefore, are highly desirable. In this study, titanium (Ti) substrates were fabricated deposited with different amounts of copper (Cu) using polydopamine (PDA)-based chemical modification technology. *In vitro*, Ti implants that were treated with PDA and deposited with Cu (Ti-PDA-Cu) showed excellent antibacterial performance against both *S. aureus* and *E. coli* compared with pristine Ti. They also markedly promoted adhesion and spreading of MC3T3-E1 cells, implying good biocompatibility of such Ti-PDA-Cu materials. *In vivo*, results from an animal model of implant-related osteomyelitis clearly demonstrated that Ti-PDA-Cu implants not only effectively inhibited bacterial infection, but also promoted osseointegration at the bone/implant interface. Taken together, these findings show that Ti-PDA-Cu possesses outstanding biocompatibility and antibacterial activity, and are candidate materials for preventing periprosthetic infection.

Received 13th September 2017
Accepted 16th October 2017

DOI: 10.1039/c7ra10203h

rsc.li/rsc-advances

1. Introduction

Titanium (Ti) and its alloys are widely used as orthopedic implant materials because of their superior properties including high corrosion resistance, considerable mechanical strength, and outstanding biocompatibility.[1,2] However, implant-associated infections often accompany common orthopedic surgeries such as internal fixation of fractures or total joint arthroplasty.[3–5] Bacterial infection and colonization on implant surfaces and subsequent biofilm formation are considered to be the main causes of serious complications.[6] Once biofilms have formed on implant surfaces, it becomes difficult to eradicate the adhered bacteria as they have reduced sensitivity toward immune responses and systemic antibiotic therapies.[7] Prolonged infection and inflammation reaction (osteomyelitis) can also lead to bone destruction (osteolysis) around the implants, which impairs implant osseointegration and may result in loss of implant stability.[8,9] Consequently, implant removal and/or repeated surgeries are often inevitable, resulting in extended hospitalization with a heavy socioeconomic burden.[10,11] Therefore, design of implant surfaces that can effectively clear bacterial infection and promote osseointegration is highly desirable (Scheme 1).

Recently, copper (Cu) and its ionic compositions have attracted attention because of their excellent antibacterial

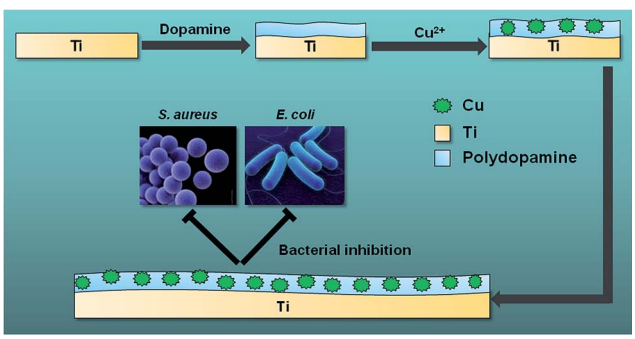

Scheme 1 Schematic of preparation of Ti-PDA-Cu substrate for bacterial inhibition.

[a]*Department of Orthopaedic Surgery, The First Affiliated Hospital, Orthopaedic Institute, Soochow University (South Campus), 188 Shizi St, 708 Renmin Rd, Suzhou, Jiangsu 215006, China. E-mail: sun_junying@hotmail.com; binli@suda.edu.cn; Fax: +86-512-6778-1163; Tel: +86-512-6778-0101; +86-512-6778-1163*

[b]*College of Chemical Engineering, Nanjing University of Science and Technology, Nanjing 210094, Jiangsu, China. E-mail: xingxiaodong07@njust.edu.cn; Tel: +86 025 84315514*

[c]*Department of Materials Science and Engineering, University of California, Los Angeles, CA, USA*

[d]*China Orthopaedic Regenerative Medicine Group (CORMed), Hangzhou, Zhejiang, China*

† These authors contributed equally to this study.

properties and superior biological activity. Cu possesses a broad spectrum against microorganisms such as *S. aureus*, *E. coli*, *S. enterica*, *C. jejuni*, and *M. tuberculosis*.[12–15] Appropriate doses of Cu have also been shown to promote various regenerative processes such as angiogenesis and osteogenesis.[15,16] Burghardt *et al.* revealed the dual functions of Cu ions, which promoted bone regeneration at lower concentration and prohibited bacterial infections at higher concentration.[17] Compared with ions such as Ag^{+}, Zn^{2+}, Co^{2+}, Al^{3+}, and Hg^{2+}, Cu^{2+} delivered the best compromise between antibacterial effectiveness and cytotoxicity.[18] As a result, Cu is considered an effective antibacterial component for incorporation within various biomaterials.[19–22] For example, Wu *et al.* found that Cu-containing mesoporous bioactive glass scaffolds showed angiogenic, osteo-stimulating and antibacterial activities, which facilitated bone defect repair.[15] Li *et al.* found that biodegradable Mg–Cu alloy implants inhibited expression of biofilm-associated and antibiotic-resistant genes, and suppressed formation of biofilm.[23] Therefore, Cu may be a useful supplement to endow implants both anti-microbial and regenerative capability. However, while it has been proven that Cu can promote bone regeneration at lower concentration and inhibit bacterial infection at higher concentration *in vitro*,[17] its possible simultaneous antibacterial activity and bone repair capacity requires further investigation *in vivo* using an infection animal model.

To date, a variety of approaches for surface modification of metal implants, including plasma spraying,[24,25] direct ion implantation,[26] magnetron sputtering,[27] plasma immersion ion implantation,[28,29] oxidation,[30] and covalent bonding,[31,32] have been developed to achieve enhanced biological activities. However, most of these approaches require special equipment or complicated procedures. In contrast, polydopamine (PDA) coating, inspired by the adhesive protein of marine mussels, has been explored as a versatile technique for surface functionalization of materials.[33,34] Under defined conditions, dopamine can undergo oxidative self-polymerization, creating a thin polymerized coating layer *via* covalent and non-covalent bonding on a wide range of materials, including metals, polymers, oxides, semiconductors and ceramics, regardless of their chemical and physical properties.[35] PDA coatings have been shown to promote cell adhesion, spreading, proliferation, and even mineralization.[36,37] Moreover, PDA can participate in reduction reactions with noble metal ions under basic conditions.[38] For example, Lee *et al.* found that PDA coating had sufficient reduction capacity in solution and required no other reducing agents for reduction of silver (Ag) ions.[39] Recently, Wu *et al.* showed that PDA/Ag nanocomposite particles have excellent biocompatibility and robust antibacterial capability, making them promising antibacterial materials for future biomedical applications.[40] Many studies have shown that PDA can be used to successfully immobilize metal ions (*e.g.* Ti^{4+}, Fe^{3+}, Cu^{2+}).[41,42] These studies have highlighted the advantages of PDA-based chemical modification technology, including ease-of-use, versatility, and high stability under physiological conditions.

The present study aimed to prepare Cu-functionalized Ti substrates using PDA coating technology to achieve both antimicrobial and osseointegration properties under simulated periprosthetic infection conditions. Various PDA-coated Ti substrates were prepared functionalized with different amounts of Cu, and *in vitro* studies were conducted to examine the antibacterial activity and biocompatibility of these materials. *In vivo*, their antibacterial and osseointegration performance in the presence of *S. aureus* was evaluated using a model of implant-related osteomyelitis in the tibia of rats. Many previous studies have focused on the interaction between *S. aureus* and osteoblasts, with the interplay between *S. aureus* and osteoclasts being much less explored. Therefore, this study also considered the direct effect of *S. aureus* on osteoclast activity *in vivo*.

2. Materials and methods

2.1 Sample preparation

Ti disks (99.6% purity) with diameters of 5.8 and 13 mm, and thickness of 1 mm were used in this study. For *in vivo* experiments, pure Ti rods of 10 mm length and 1.2 mm diameter were used. These materials were supplied by Tianjin Zhengtian Medical Device Company (Tianjin, China). Prior to PDA coating, Ti disks and rods were first ultrasonically cleaned stepwise using acetone, ethanol, and deionized water. Then the cleaned disks and rods were air-dried and stored in a desiccator to avoid contamination. Dopamine solutions were prepared by dissolving dopamine (Sigma, MO) at a concentration of 2 mg mL^{-1} in 10 mM Tris–HCl buffer solutions (pH = 8.5). The Ti disks and rods were then soaked in the dopamine solution overnight for PDA coating. The PDA-coated Ti substrates (Ti-PDA) were collected and ultrasonically cleaned using deionized water and air-dried at room temperature. Cu ions were immobilized in PDA coating *via* the soaking method. $CuCl_2$ (Adama Reagent Co. Ltd. Shanghai, China) was mixed with deionized water to prepare solutions with different Cu concentration of 0.02 mmol L^{-1}, 0.1 mmol L^{-1} and 0.5 mmol L^{-1}. Then the Ti-PDA samples were immersed in the different Cu solutions for 1 h to anchor Cu onto the surface, with the products named as Ti-PDA-Cu 0.02, Ti-PDA-Cu 0.1, and Ti-PDA-Cu 0.5, respectively. Pure Ti was used as a control group. The samples were then ultrasonically cleaned using deionized water and air-dried. All the samples were sterilized by irradiation before further experiments.

2.2 Surface characterizations

Scanning electron microscopy (SEM, S-3400, Hitachi, Tokyo, Japan) was used to study the surface morphology of the samples. The surface chemistry of the samples was examined qualitatively using X-ray photoelectron spectroscopy (XPS, PHI 5802, Physical Electronics, London, UK). The Cu, N, C, O, and Ti profiles were acquired by XPS in conjunction with argon ion bombardment at a sputtering rate of about 4 nm min^{-1}. Surface wettability was assessed using a tensiometer (Kruss, Germany). Distilled water was used as the media and three replicates were performed on each specimen for statistical accountability.

2.3 Release of Cu ions

The Ti-PDA-Cu 0.02, Ti-PDA-Cu 0.1, and Ti-PDA-Cu 0.5 samples were immersed in 3.5 mL phosphate buffer saline (PBS,

Hyclone, Utah, USA) solution at 37 °C for 7 days. The released amount of Cu^{2+} ions from different Ti-PDA-Cu samples was measured at 1, 2, 4, 8, 12 hours and from 1 to 7 days using an Ultraviolet Spectrophotometer (TU-1900, Persee, Beijing, China). At each time point, 3 mL of immersion solution was taken out for analysis and the solution was filled up with the same volume of PBS. The cumulative release amount of Cu ions was calculated as the sum of released Cu ions from each sample within different immersion time intervals. Three replicates were used for each group.

2.4 Cell culture

MC3T3-E1 mouse preosteoblasts (CRL-2594, subclone 14, ATCC) were cultured in α-minimum essential medium (α-MEM, Gibco, Grand Island, New York, USA) supplemented with 10% fetal bovine serum (Gibco) and 1% penicillin/streptomycin at 37 °C in a 5% CO_2 environment. The media were refreshed every 3 days. When cells reached confluence, a trypsin–EDTA solution (0.5 g L^{-1} trypsin and 0.2 g L^{-1} EDTA, Gibco) was used to detach cells from the bottom of the culture flasks, and one-third of the total cells were transferred into a new tissue culture flask. Cells were then seeded onto the different experimental substrates. Disks of diameter 5.8 mm were placed on 96-well polystyrene plates with an initial density of 1×10^4 cells per well. The 13 mm disks were placed on 24-well polystyrene plates at a concentration of 2×10^4 cells per well.

2.5 Cell morphology observation

MC3TE-E1 cells were cultured on the surfaces of disks of diameter 5.8 mm for 24 h. After washing with PBS, the samples were fixed in 2.5% glutaraldehyde (Sigma, St. Louis, MO, USA) in PBS for 1 h and then rinsed three times with PBS for 10 min. After that, the cells were dehydrated in a graded series of ethanol concentrations (30%, 50%, 70%, 90% and 100%) for 30 min each and left in 100% ethanol. The samples were dried using a Critical Point Dryer (CPD030, Leica, Wetzlar, Germany) and sputter-coated gold using an Ion Sputter (SC7620, Quorum Technologies, Lewes, UK) prior to SEM examination. The morphology of cells on surface of disks was observed by SEM (SEM, S-3400, Hitachi, Tokyo, Japan).

2.6 Cytoskeletal observation

Each material was incubated with 2×10^4 cells for 24 h. The cells were fixed with 4% paraformaldehyde in PBS for 15 min at room temperature. The cells were then washed twice using PBS and permeabilized with 0.2% Triton X-100. After that, they were incubated with FITC-labeled phalloidin (5 μg mL^{-1} in PBS) containing 1% BSA for 1 h at room temperature. The cell nuclei were then stained with DAPI. Finally, cell morphology and cytoskeletal arrangement were observed using an EVOS fluorescence microscope (AMG, Thornwood, NY, USA).

2.7 Cell viability assays

CCK-8 cell viability assay was conducted according to the manufacturer's protocol (CCK-8, Dojindo Laboratories, Tokyo, Japan). In brief, 100 μL cell suspension with a cell concentration of 1×10^4 mL^{-1} was pipetted into a 96-well plate and cultivated at 37 °C with 5% CO_2 in air for 1, 3, 5, 7 days, respectively. At predetermined time points, the samples were washed three times with PBS to remove non-viable cells. Then 10 μL CCK-8 reagent was added to each sample and incubated at 37 °C for 2 h. After that, the yellow supernatant was pipetted into a microplate and the absorbance was measured at 450 nm using a microplate reader. Three duplicates were used for each sample. The cell viability was expressed by relative growth rate (RGR), which was calculated as follows.

$$\mathrm{RGR} = (\mathrm{OD}_{\mathrm{sample}}/\mathrm{OD}_{\mathrm{blank}}) \times 100\%$$

where OD_{sample} is the optical density of the Ti, Ti-PDA, Ti-PDA-Cu samples and OD_{blank} is the optical density of blank control sample (α-MEM medium). A material with cytotoxicity of Grade 0 or Grade 1, *i.e.*, RGR of 90–100% and 75–90%, respectively, has no toxicity to cells and can be considered as biocompatible.

2.8 *In vitro* antibacterial tests

The antibacterial property of samples was investigated by a bacteria counting method using both *S. aureus* and *E. coli*. The samples were first sterilized in 75% ethanol for 2 h and rinsed three times with sterile PBS. Then solutions of bacteria at a concentration of 10^6 CFU mL^{-1} were dripped onto the surfaces at a density of 100 μL cm^{-2}. After 24 h of incubation at 37 °C, the dissociated bacteria were collected and inoculated onto a standard agar culture plate for 24 h. The antibacterial rate was determined as follows.

$$\text{Antibacterial rate (\%)} = (\text{CFU of control} - \text{CFU of experimental group})/\text{CFU of control} \times 100\%$$

where pristine Ti sample served as the control and Ti-PDA, Ti-PDA-Cu 0.02, Ti-PDA-Cu 0.1, and Ti-PDA-Cu 0.5 samples constituted the experimental groups.

2.9 Animal studies

Forty male SD rats (from Soochow University Animal Center) weighing from 300 to 350 g were used for *in vivo* assays. All SD rats were randomly divided into five groups (of eight) as follows; Ti, Ti-PDA, Ti-PDA-Cu 0.02, Ti-PDA-Cu 0.1, and Ti-PDA-Cu 0.5. The operation was conducted under general anesthesia induced intraperitoneally with 4% chloral hydrate (0.9 mL/100 g). The metaphysis of left tibiae was chosen as the surgical site. The operating field was shaved and sterilized with betadine scrubs. A skin incision was made over the tibial tuberosity. A longitudinal incision was made at the proximal tibial metaphysis of the tibia. To access the tibial medullary cavity, a hole was drilled using a circular drill (1.2 mm diameter) to make a channel from the proximal tibial metaphysis into the medullary canal. For bacterial inoculation, 20 μL of *S. aureus* suspension at a concentration of 10^4 CFU mL^{-1} was injected into the medullary cavity with a microsyringe. Following inoculation, sterile Ti rods (1.2 mm in diameter and 10 mm in length) were inserted into the medullary cavity until they were beneath the growth

plate. Incisions were closed by interrupted sutures with 4-0 nylon. After surgery, the rats were housed in ventilated rooms and allowed to eat and drink *ad libitum*. This study was performed in strict accordance with the NIH guidelines for the care and use of laboratory animals (NIH Publication no. 85-23 Rev. 1985) and was approved by the Institutional Animal Care and Use Committee of Soochow University (Suzhou, China).

2.10 Micro-CT evaluation

To investigate the newly formed bone at 4 weeks after surgery, the rods were scanned using high-resolution micro-computed tomography (micro-CT; Skyscan 1176, Skyscan, Belgium). Scanning was performed at 65 kV using the Al 1 mm filter with a resolution of 18 μm. The three dimensional (3D) high-resolution reconstructed images were obtained by the software provided by the manufacturer. The relevant data were obtained by analyzing the bone formation at a range of 1.4 mm around the rods.

2.11 Histological analysis and immunohistochemistry

All animals were euthanized by overdose of chloral hydrate at 2 and 4 weeks post surgery. Eight left tibiae of each group were removed and separated from the soft tissue, and fixed in 4% paraformaldehyde for 48 h. Then the proximal tibias were decalcified in ethylenediaminetetraacetic acid (EDTA) for 28 days. After that, all the Ti-rods were carefully pulled out without destroying the newly formed bone tissue, and the samples were dehydrated with graded ethanol and embedded in paraffin. Transverse sections were cut into sections (5 um thick) and then stained with hematoxylin-eosin (H&E), Masson's Trichrome staining. Osteoclasts were identified using a tartrate-resistant acid phosphatase (TRAP) staining kit (Sigma, St. Louis, MO, USA). The *S. aureus* was visualized using diaminobenzidine (DAB) staining of murine monoclonal antibody (ab37644; Abcam plc, Cambridge, UK) as previously reported.[43] Each section was examined using a Nikon 80i light microscope (Nikon Instruments, Melville, NY).

2.12 Statistical analysis

All *in vitro* experiments were performed in triplicate and the data are given as mean ± standard deviation. Statistical analysis was performed using one-way analysis of variance (ANOVA) and Student *t*-test where appropriate using Graphpad Prism software. A difference of $p < 0.05$ was considered to be statistically significant.

3. Results

3.1 Surface characterizations of Ti-PDA-Cu substrates

The surface morphology of samples was examined using SEM. There was no apparent difference among the surfaces of Ti, Ti-PDA, and Ti-PDA-Cu samples, meaning that coating with PDA and deposition of Cu did not markedly change the surface topography of the Ti samples (Fig. 1). The feature peaks of Ti, O, and C elements can be seen clearly in the XPS spectra of all the coated samples (Fig. 2). The C signal on pristine Ti sample was attributed to surface contamination. The presence of the peaks of N and Cu indicates successful coating of PDA and deposition of Cu on Ti. The content of Cu was estimated to be about 4.28%, 6.01%, and 8.47% for Ti-PDA-Cu 0.02, Ti-PDA-Cu 0.1 and Ti-PDA-Cu 0.5 samples, respectively. To examine the wettability of samples, the water contact angles were measured (Fig. 3). Compared with Ti ($80 \pm 6.76^\circ$), Ti-PDA, Ti-PDA-Cu 0.02, Ti-PDA-Cu 0.5, and Ti-PDA-Cu 0.1 samples all showed higher hydrophilicity, with contact angles of $45 \pm 2.81^\circ$, $49 \pm 4.38^\circ$, $54 \pm 4.38^\circ$ and $60 \pm 5.45^\circ$, respectively.

3.2 Release of Cu ions from Ti-PDA-Cu substrates

To study release of Cu ions from the different Ti-PDA-Cu samples, they were immersed in PBS for 7 days and the concentration of released Cu^{2+} ions was periodically monitored (Fig. 4). After the initial 24 h, Ti-PDA-Cu 0.02, Ti-PDA-Cu 0.1 and Ti-PDA-Cu 0.5 samples released 0.16 ± 0.01, 0.45 ± 0.01 and 0.84 ± 0.02 mmol L^{-1} of Cu^{2+} ions, respectively. Rapid Cu^{2+} ion release occurred at day 1. After that, release of Cu^{2+} ions gradually slowed. Compared with Ti-PDA-Cu 0.02 and Ti-PDA-Cu 0.1 samples, Ti-PDA-Cu 0.5 released many more Cu^{2+} ions at all periods of time. After immersion for 7 days, the released Cu^{2+} ions from Ti-PDA-Cu 0.5 were significantly higher than those of Ti-PDA-Cu 0.02 and Ti-PDA-Cu 0.1. The total amount of Cu^{2+} ions released in 7 days were 0.32 ± 0.01, 0.65 ± 0.01, and 1.17 ± 0.04 mmol L^{-1} for the substrates of Ti-PDA-Cu 0.02, Ti-PDA-Cu 0.1 and Ti-PDA-Cu 0.5, respectively.

3.3 Cell morphology and cytoskeletal structures

When cultured on Ti, Ti-PDA, and different Ti-PDA-Cu samples for 24 h, MC3T3-E1 pre-osteoblastic cells display different morphology (Fig. 5). The cells showed relatively round shape when cultured on Ti. However, they exhibited a much flatter shape on the surfaces of Ti-PDA and Ti-PDA-Cu samples with different Cu contents, which could be attributed to enhanced biocompatibility from the PDA coating. Further, the cytoskeletal structures of MC3T3-E1 cells cultured on different samples were examined using fluorescence microscopy (Fig. 6). Cells adhered well on these samples, as indicated by the well-spreading cytoplasm and development of numerous lamellipodia and filopodia processes. The cells cultured on Ti substrates were not fully spread and showed relatively round morphology which seemed to lack microfilaments. However, on Ti-PDA and different Ti-PDA-Cu substrates the cells exhibited much flattened and irregular morphology, implying stronger cell adhesion on the samples. The actin filaments seemed to be better developed within the cells on Ti-PDA and Ti-PDA-Cu substrates than in those on Ti substrates.

3.4 Cell proliferation

The proliferation of MC3T3-E1 cells on Ti, Ti-PDA and different Ti-PDA-Cu substrates was studied using CCK-8 assays. The results clearly show that the number of cells steadily increased within 7 days of culture for all five groups (Fig. 7A). At day 1, cell proliferation on Ti substrates was superior to that on Ti-PDA and different Ti-PDA-Cu substrates. No significant difference

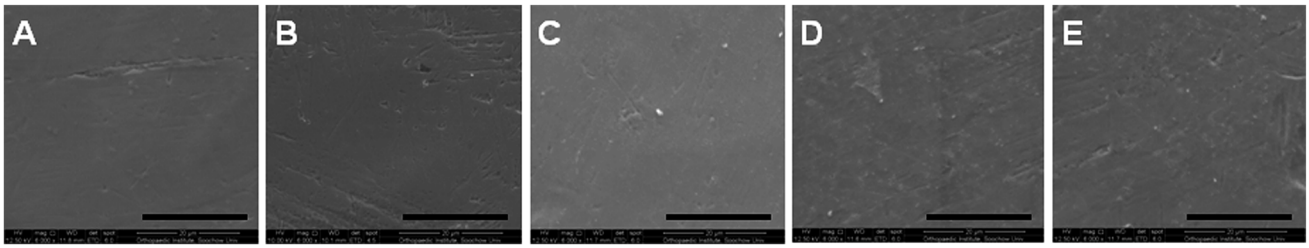

Fig. 1 SEM images of Ti (A), Ti-PDA (B), Ti-PDA-Cu 0.02 (C), Ti-PDA-Cu 0.1 (D), and Ti-PDA-Cu 0.5 (E) substrates. Scale bars, 20 μm.

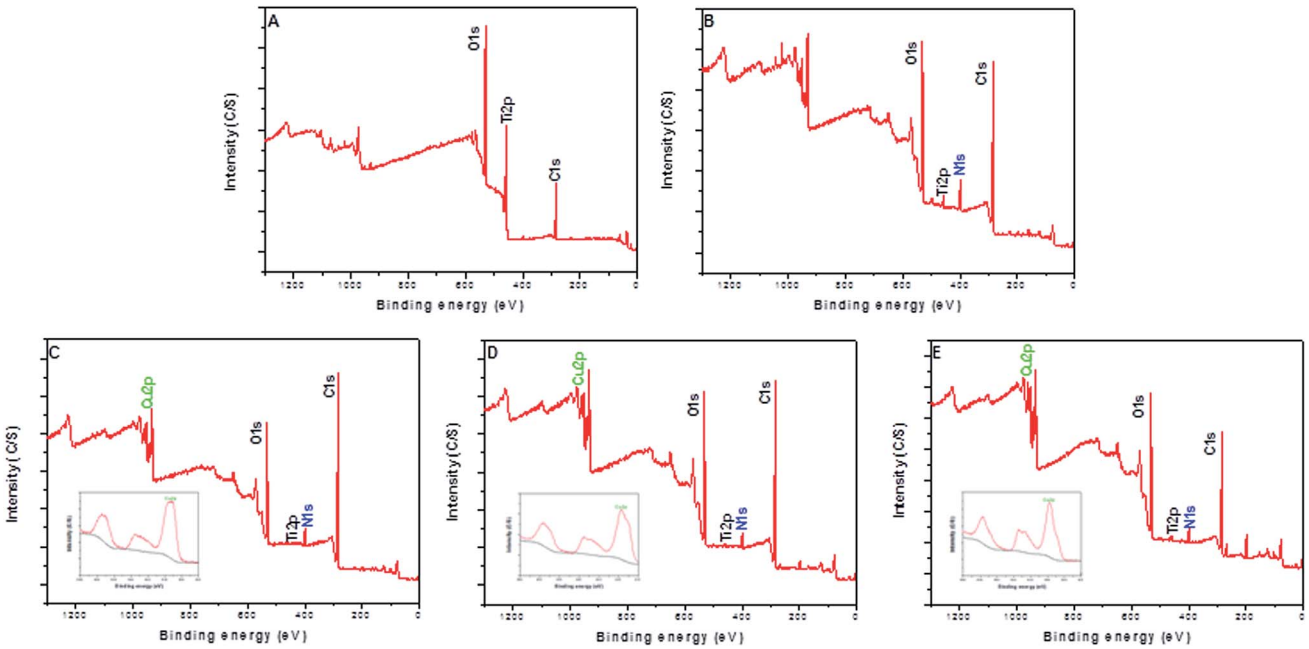

Fig. 2 XPS survey spectra of Ti (A), Ti-PDA (B), Ti-PDA-Cu 0.02 (C), Ti-PDA-Cu 0.1 (D), and Ti-PDA-Cu 0.5 (E) substrates. The insets in (C–E) show the high-resolution spectra of Cu 2p.

existed between the Ti-PDA and different Ti-PDA-Cu groups. At day 3, the cell numbers were much lower for Ti-PDA and different Ti-PDA-Cu 0.02 substrates, compared with Ti substrates. In addition, cell numbers were lower for Ti-PDA-Cu 0.1 and Ti-PDA-Cu 0.5 substrates compared with Ti substrates. Upon 5 days of culture, cell proliferation on Ti substrates was markedly higher than that on different Ti-PDA-Cu substrates. Cell proliferation on Ti-PDA substrates was also lower than that on Ti. However, after 7 days of culture, no differences could be found in OD values among Ti, Ti-PDA, and different Ti-PDA-Cu substrates. The calculated RGRs of MC3T3-E1 cells on different samples at different culture times were all higher than 75%, meaning that Ti-PDA, and Ti-PDA-Cu with various Cu contents all possess good biocompatibility, as does Ti (Fig. 7B).

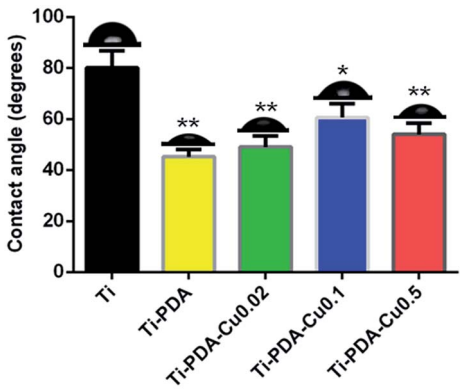

Fig. 3 Water contact angles of Ti, Ti-PDA, and Ti-PDA-Cu substrates. *$p < 0.05$; **$p < 0.01$.

3.5 *In vitro* antibacterial property

The antibacterial activity of Ti-PDA and different Ti-PDA-Cu substrates was tested against *S. aureus* and *E. coli*. The bacteria were incubated on the samples for 24 h and the viable bacteria were then detached and re-cultivated on agar plates to count the colonies. The number of bacterial colonies decreased with Cu content on Ti-PDA-Cu substrates (Fig. 8). On Ti, Ti-PDA, and Ti-PDA-Cu 0.02 samples, there were a large number of bacterial colonies, which indicates that the samples did not

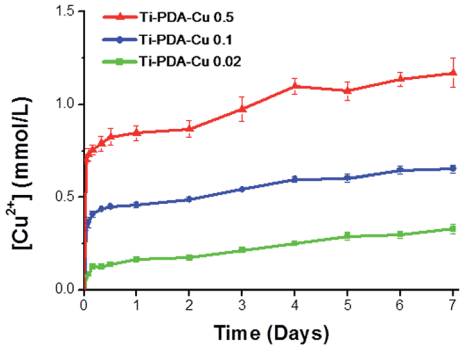

Fig. 4 Cumulative release profiles of Cu^{2+} ions from Ti-PDA-Cu substrates on immersion in PBS at 37 °C.

effectively impede the survival of bacteria. In contrast, fewer colonies were found on Ti-PDA-Cu 0.1 and Ti-PDA-Cu 0.5 samples, suggesting that high Cu concentration effectively inhibited the survival and growth of bacteria. The antibacterial rates of Ti-PDA and different Ti-PDA-Cu substrates against *S. aureus* and *E. coli* were quantitatively referenced to Ti. As shown in Fig. 9, the average antibacterial rates against *S. aureus* of Ti-PDA-Cu 0.5 and Ti-PDA-Cu 0.1 are 99.4% and 91.9%, which are remarkably higher than the 41.5% for Ti-PDA-Cu 0.02 and 10.2% for Ti-PDA substrates. A similar tendency was observed for *E. coli*, with the average antibacterial rates measured to be 11.9%, 46.2%, 92.3% and 98.3% for Ti-PDA, Ti-PDA-Cu 0.02, Ti-PDA-Cu 0.1, and Ti-PDA-Cu 0.5, respectively.

3.6 Micro-CT evaluation

Fig. 10A shows 3D reconstructed micro-CT images of the five implanted samples at 4 weeks after surgery. Little bone was found around Ti and Ti-PDA implants. However, more bone could be observed around the Ti-PDA-Cu 0.02 implant, and the highest amount of newly formed bone was seen in images of Ti-PDA-Cu 0.1 and Ti-PDA-Cu 0.5. Fig. 10B shows the calculated bone volume to tissue volume (BV/TV) under the same threshold and volume interest (VOI) for CT scanning. Notably,

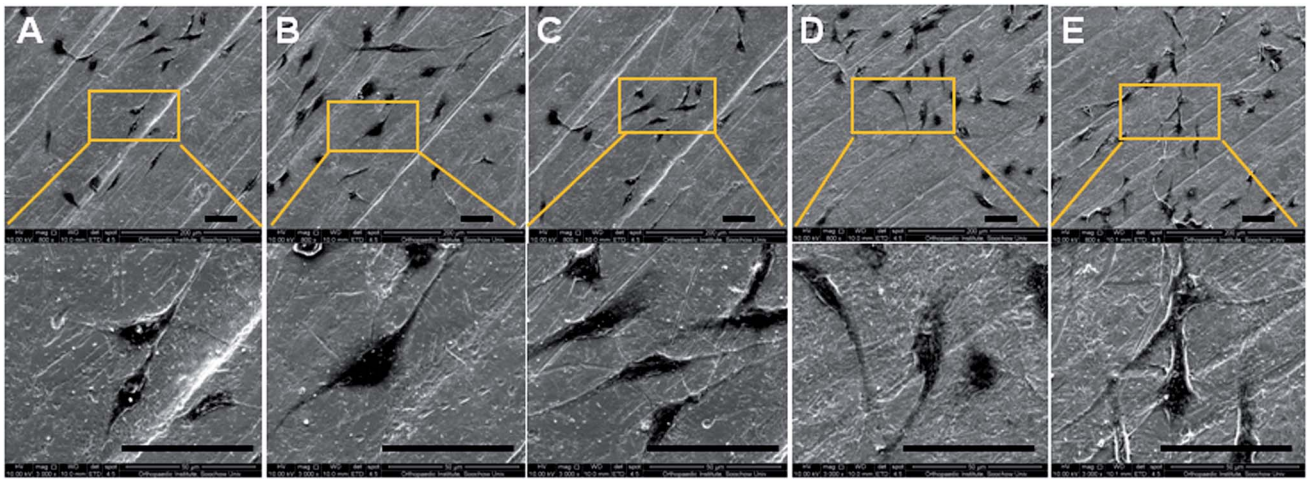

Fig. 5 Morphology of MC3T3-E1 cells cultured on Ti (A), Ti-PDA (B), Ti-PDA-Cu 0.02 (C), Ti-PDA-Cu 0.1 (D), and Ti-PDA-Cu 0.5 (E) substrates for 24 h as observed using SEM. Scale bars, 200 μm.

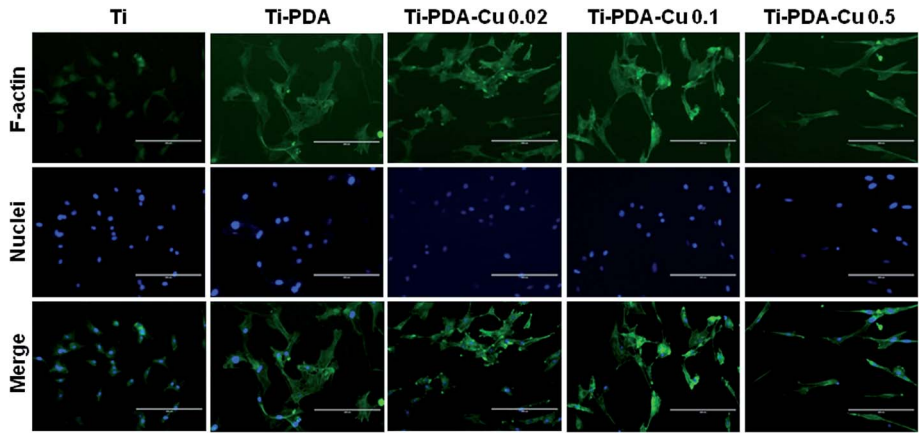

Fig. 6 Immunofluorescence images of MC3T3-E1 cells after being cultured on Ti, Ti-PDA, Ti-Cu 0.02, Ti-PDA-Cu 0.1, and Ti-PDA-Cu 0.5 substrates for 24 h. The actin filaments were stained with FITC-labeled phalloidin (green) and nuclei were stained with DAPI (blue). Scale bars, 200 μm.

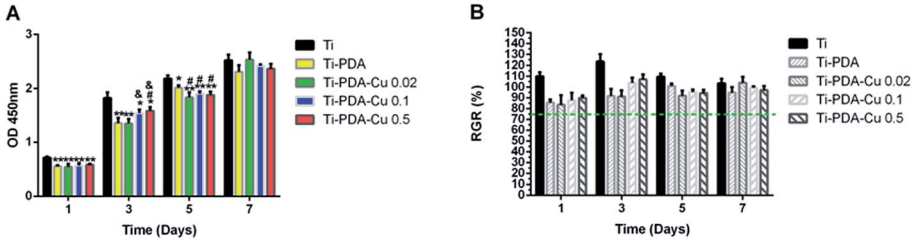

Fig. 7 Proliferation of MC3T3-E1 cells on Ti, Ti-PDA, Ti-PDA-Cu 0.02, Ti-PDA-Cu 0.1, and Ti-PDA-Cu 0.5 substrates. (A) OD values in CCK-8 tests; (B) RGR values. Cells cultures on Ti substrates were used as control. $^{**}p < 0.01$ and $^{*}p < 0.05$ *vs.* Ti; $^{\#}p < 0.05$ *vs.* Ti-PDA; and $^{\&}p < 0.05$ *vs.* Ti-PDA-Cu 0.02.

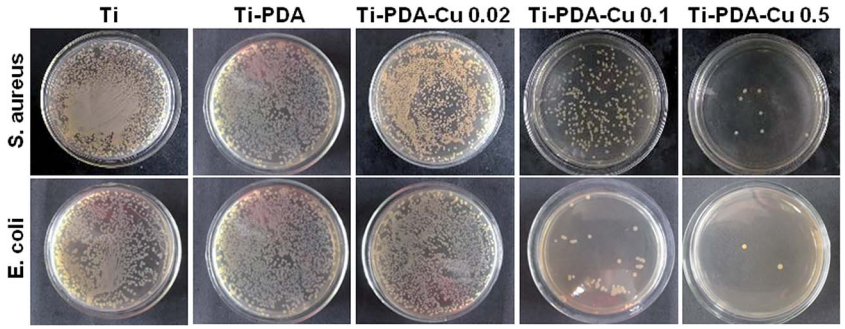

Fig. 8 Re-cultivated *S. aureus* and *E. coli* colonies collected from different substrates that were previously implanted *in vivo*. Culture time, 1 day.

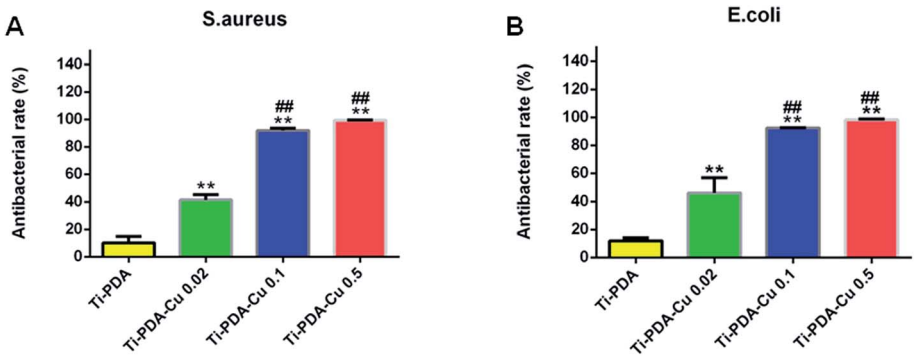

Fig. 9 Antibacterial rates of Ti-PDA, Ti-PDA-Cu 0.02, Ti-PDA-Cu 0.1, and Ti-PDA-Cu 0.5 substrates against *S. aureus* (A) and *E. coli* (B) after 24 h re-cultivation. $^{**}p < 0.01$ *vs.* Ti-PDA, and $^{\#\#}p < 0.01$ *vs.* Ti-PDA-Cu 0.02.

Ti-PDA-Cu 0.1 and Ti-PDA-Cu 0.5 rods exhibited the highest percentage of BV/TV, indicating the best performance of osseointegration among these groups.

3.7 Histological analysis and immunohistochemistry

H&E and Masson's trichrome staining were used to evaluate bacterial infection and osseointegration *in vivo*. H&E staining images of the five groups are presented in Fig. 11. Numerous neutrophils emerged around the tibia medullary cavity in the Ti, Ti-PDA, and Ti-PDA-Cu 0.02 groups, suggesting that bacterial infection occurred during the 2 weeks. Many chronic inflammatory cell infiltrations were also observed after 4 weeks. In contrast, no sign of infection was seen in the Ti-PDA-Cu 0.1 and Ti-PDA-Cu 0.5 groups. Newly formed bone at the bone/implant interface was evaluated by Masson's trichrome staining (Fig. 12). At week 2, fibrous tissue was seen at the bone/implant interface in the Ti-PDA-Cu 0.1 and Ti-PDA-Cu 0.5 groups. After 4 weeks, a large amount of woven bone with diminishing fibrous tissue was observed at the bone/implant interface in the Ti-PDA-Cu 0.1 and Ti-PDA-Cu 0.5 groups. As a comparison, new bone tissue could hardly be found for the other groups. Osteoclast activity was identified based on tartrate-resistant acid phosphatase (TRAP) staining (Fig. 13). Typical signs of bone resorption could be clearly seen, as indicated by accumulation of osteoclasts around Ti, Ti-PDA, and Ti-PDA-Cu 0.02 samples at 2 weeks. However, the number of osteoclasts decreased after 4 weeks. In contrast, there was no sign of osteoclasts for the Ti-PDA-Cu 0.1 and Ti-PDA-Cu 0.5 groups, suggesting that

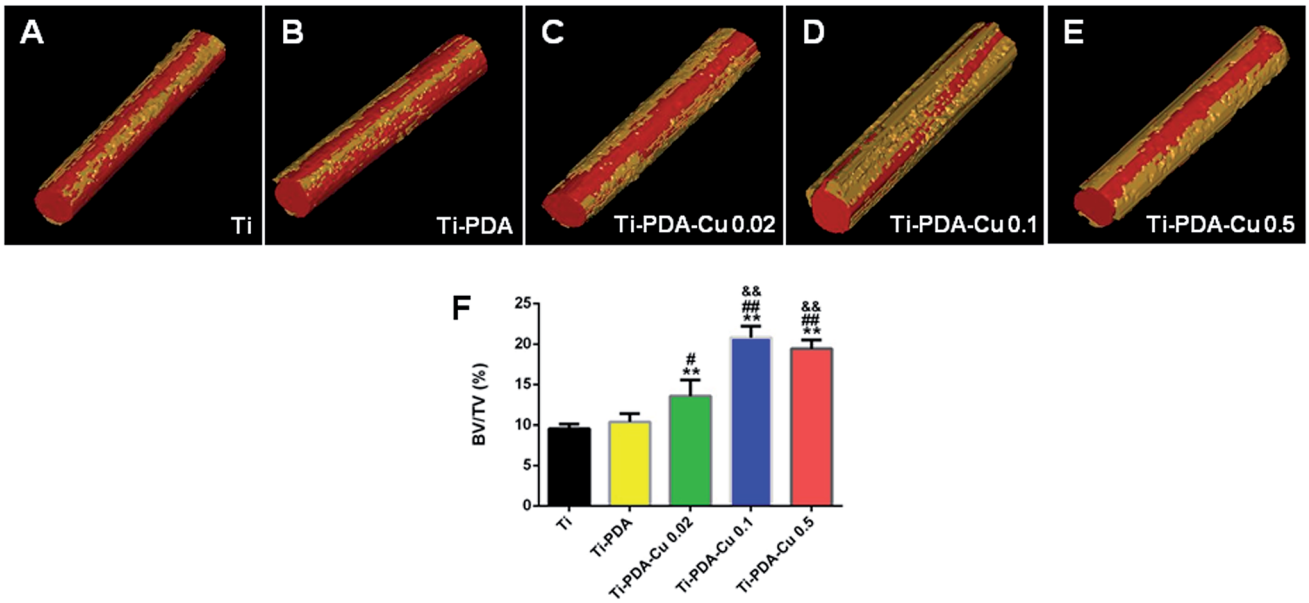

Fig. 10 Reconstructed 3D models showing bone formation on Ti (A), Ti-PDA (B), Ti-PDA-Cu 0.02 (C), Ti-PDA-Cu 0.1 (D), and Ti-PDA-Cu 0.5 (E) substrates at 4 weeks post-implantation. (F) The peri-implant bone formation quantified according to the percentage bone volume (BV) among tissue volume (TV) (BV/TV). $^{**}p < 0.01$ *vs.* Ti, $^{\#}p < 0.05$ and $^{\#\#}p < 0.01$ *vs.* Ti-PDA, $^{\&\&}p < 0.01$ *vs.* Ti-PDA-Cu 0.02.

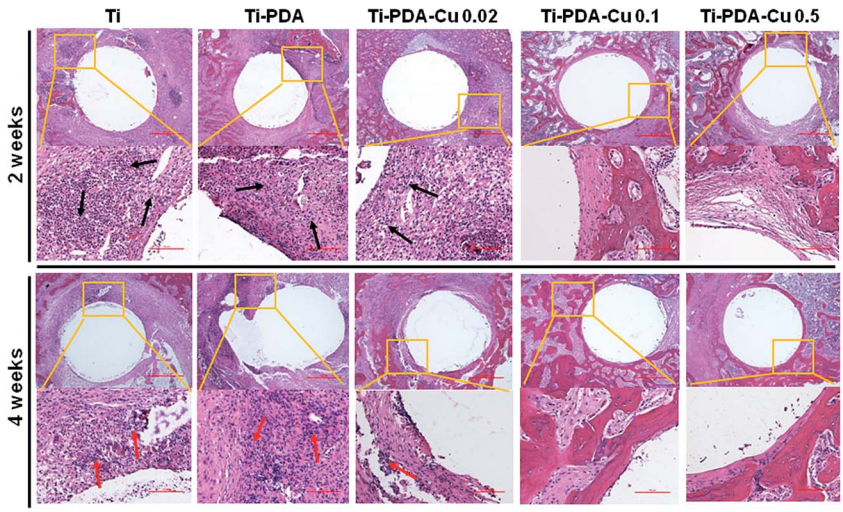

Fig. 11 H&E staining of tissues surrounding various implants at 2 and 4 weeks post implantation. Scale bars, 500 μm.

negligible bone resorption occurred in these cases. Finally, the inoculated *S. aureus* was visualized using immunohistochemical analysis (Fig. 14). Despite the same initial number of bacteria upon cultivation, there were evidently abundant bacteria in the Ti, Ti-PDA, Ti-PDA-Cu 0.02 groups 2 weeks after surgery, whereas only a trace number of bacteria was found in the Ti-PDA-Cu 0.1 group and no bacteria was found for Ti-PDA-Cu 0.5. The bacteria were primarily located at the center of the inflammation. After 4 weeks, bacterial infection could be evidently observed in Ti, Ti-PDA, Ti-PDA-Cu 0.02 groups. However, no bacterial survival, either as single organisms or in colonies, could be detected in the Ti-PDA-Cu 0.1 and Ti-PDA-Cu 0.5 groups.

4. Discussion

Implanted biomaterials play a key role in successful fixation of bone fractures, spinal reconstruction, joint arthrodesis, total joint arthroplasty, and many other orthopedic applications.[1,11,25,44,45] However, implant-related infection is one of the most severe complications of reconstructive orthopedic surgery. Of the infectious bacteria, *Staphylococcus aureus* (*S. aureus*) is one of the most prevalent causative pathogens inducing bone infection (osteomyelitis).[8,46] Periprosthetic infection and osteomyelitis rates of total hip and total knee arthroplasties have been reported to reach about 1%, but accounted for more than 25% of revision surgery.[10,23] Moreover, about 10% of surgical revision

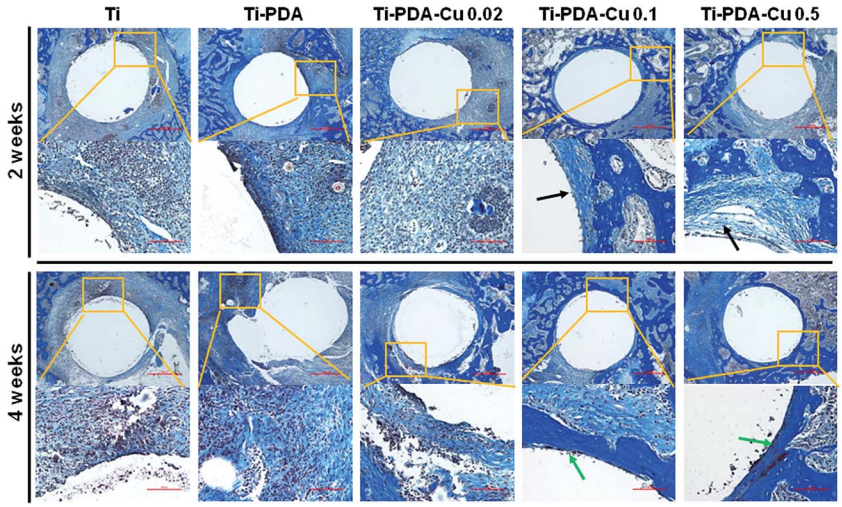

Fig. 12 Masson's trichrome staining of tissues surrounding various implants at 2 and 4 weeks post implantation. Scale bars, 500 μm.

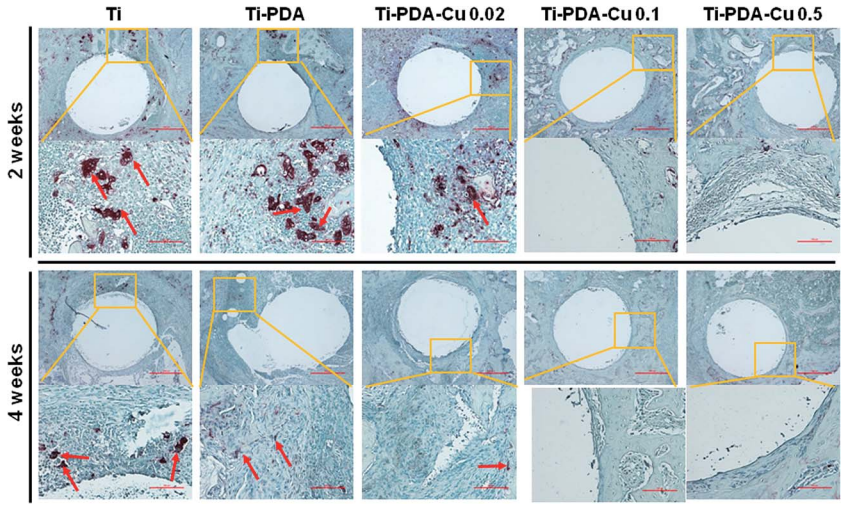

Fig. 13 TRAP staining of tissues surrounding various implants at 2 and 4 weeks post implantation. Scale bars, 500 μm.

procedures for infected hip prostheses experienced re-infection within 2 years.[47] Therefore, for a successful implant, to win "the race for the surface" tissue integration must occur prior to viable bacterial adhesion, thereby inhibiting colonization of bacteria on the surface of implants.[48] Thus, preventing infection and promoting osseointegration are the most desirable features for ideal implantable biomaterials, and ultimately determine the long-term success of implants.[49] From the perspective of clinical applications, the ideal implanted biomaterial against prophylaxis periprosthetic infection must meet various requirements. First, the implant biomaterial must have long-term continuous antibacterial effects without exhibiting toxicity to eukaryotic cells, as periprosthetic infection debridement surgery always leaves residual bacteria in the bone tissue, and conventional implant after revision surgery can lead to a high recurrence rate of infection. Second, it must exhibit broad-spectrum antibacterial performance as periprosthetic infections are often caused by various bacterial species, both Gram-positive and Gram-negative. Third, the implanted biomaterial must perform two biological activities, promoting osseointegration and inhibiting osteoclast activity caused by infection, because implant-related osteomyelitis can lead to bone damage around the prosthesis and may finally contribute to implant loosening.[8,9,29,50]

In this study, Ti substrates were functionalized with PDA coating and Cu ions to achieve both biocompatibility and antibacterial performance. The Cu ions were anchored inside the PDA coating through coordination interaction, and sustained release of Cu ions was observed. To determine the antibacterial properties of different Ti substrates, *S. aureus* and *E. coli* were utilized as model bacteria as implanted biomaterials often face infections from a wide variety of Gram positive and Gram negative bacteria.[51] The present results clearly demonstrate that the antibacterial rates of the different Ti-PDA-Cu samples evidently improved with the increment of Cu content, in which the Ti-PDA-Cu 0.5 and Ti-PDA-Cu 0.1 groups exhibited the best antibacterial activity against both *S. aureus* and *E. coli*

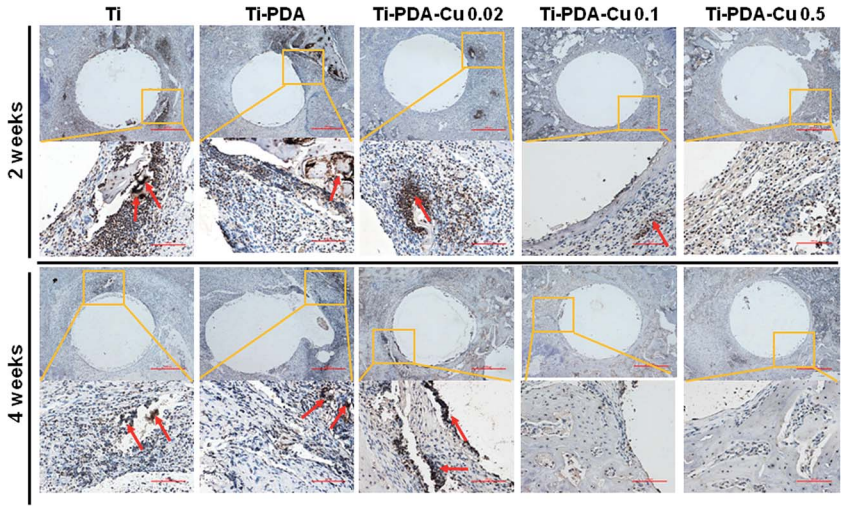

Fig. 14 Immunohistochemical staining of tissues surrounding various implants at 2 and 4 weeks post implantation. Scale bars, 500 μm.

after 24 h (Fig. 8 and 9). This is in accordance with a number of studies which show that the antibacterial activity of Cu or Cu-modified surface is closely related to the Cu content.[17,21] At the same time, the Cu^{2+} ions release assay showed that the Cu^{2+} ion concentration increased with extension of the immersion time (Fig. 4). Previous studies revealed that increased influx of Cu^{2+} into bacteria generated reactive oxygen species, which could destroy the integrity of cytoplasmic membrane, inhibit respiration, and cause DNA degradation.[52,53] Du *et al.* reported that the minimal inhibitory concentration (MIC) of Cu ion against *S. aureus* and *E. coli* was 448 μg mL^{-1} and 256 μg mL^{-1}, respectively.[54] Burghardt *et al.* showed that when Cu concentration was 0.8 mM, planktonic *S. aureus* could be completely cleared and no re-growth was found with 4 days.[17] In our case, it is believed that the released Cu^{2+} ions effectively inhibited the bacteria in contact with the surface of Ti-PDA-Cu substrates.

Cu is a trace element in the human body, and low-level Cu is essential as a cofactor for enzymes and metalloproteins.[23] However, excess Cu intake can be harmful to the human body, causing inhibition of cell growth, tissue injury and disease. Thus, biocompatibility of a biomaterial must be considered before its clinical application. In this study, MC3T3-E1 cells, mouse preosteoblasts, were used for the cytocompatibility assay. Contact and interaction between cells and biomaterial surfaces are important physiological processes affected by the biocompatibility of materials. SEM images showed that cells adhered well to the surface of different Ti substrates (Fig. 5). The cells had relatively round morphology on Ti, whereas they exhibited a much flatter irregular shape on the surfaces of Ti-PDA and different Ti-PDA-Cu samples. Consistent with the fluorescence microscopy results (Fig. 6). MC3T3-E1 cells adhered well on these surfaces, as demonstrated by the well spreading cytoplasm and development of numerous lamellipodia and filopodia processes. The cells cultured on Ti substrates showed relatively round morphology which seemed to lack microfilaments. In contrast, MC3T3-E1 cells exhibited a much flatter and irregular morphology on Ti-PDA and different Ti-PDA-Cu substrates, which suggested better development of actin filaments within MC3T3-E1 cells. These results are in line with previous studies and revealed that PDA-coated Ti surfaces could promote cell adhesion and spreading. Furthermore, the quantitative CCK-8 and RGR results clearly proved the non-cytotoxicity of different Ti substrates (Fig. 7). MC3T3-E1 cell proliferation on Ti-PDA and different Ti-PDA-Cu substrates were slightly lower than that on Ti substrates at 1, 3, 5 days, but no difference was found in OD values among Ti, Ti-PDA, and Ti-PDA-Cu substrates after 7 days of culture. The cytotoxicity scale is ranked as Grade 0 for Ti substrates, and Grade 1 for Ti-PDA and different Ti-PDA-Cu samples at all incubation time points. Previously, Cortizo *et al.* reported a 40–50% decrease in surviving MC3T3-E1 cells at 104 μg mL^{-1} Cu^{2+} ions.[55] The present results indicate that all the Ti-PDA-Cu substrates did not show apparent cytotoxicity to MC3T3-E1 cells, which might be attributed to relatively lower Cu ion concentration. Zhang *et al.* reported that Cu content up to 25 wt% in Ti–Cu alloys has no cytotoxicity to MG63 cells.[56] In addition, the total body Cu in adults is approximately 80 mg and the acceptable daily intake is suggested to be 1.3–8.0 mg per day by the World Health Organization (WHO).[57] Based on the above results, it is believed that Ti-PDA-Cu 0.1 and Ti-PDA-Cu 0.5 successfully combine the functionalities of both excellent antibacterial effects and good cell biocompatibility.

An intramedullary implant approach was chosen that mimics periprosthetic infection of total joint replacements to evaluate the performance of the implants *in vivo*. At 2 weeks post surgery, typical signs of numerous neutrophils exudate in the tibia medullary cavity and osteoclasts emerged near the trabecular bone in Ti, Ti-PDA and Ti-PDA 0.02 groups, demonstrating the presence of bacterial infection and bone resorption.[58,59] The immunohistochemical analysis also showed similar results, which were in line with the antibacterial experiment *in vitro*. In the Ti-PDA-Cu 0.1 and Ti-PDA-Cu 0.5 groups, fibrous tissues were detected at the bone/implant interface, which indicated inhibition of infection and

stimulation of new bone formation. After 4 weeks, the presence of osteomyelitis in the Ti, Ti-PDA and Ti-PDA 0.02 groups was confirmed by histological analyses on tibiae, including chronic inflammatory cell infiltration, osteoclastic bone resorption, and extracellular bacteria surrounding the implants.[60] On the contrary, no sign of bacterial infection and bone resorption was found in the Ti-PDA-Cu 0.1 and Ti-PDA-Cu 0.5 groups. Moreover, a large amount of woven bone with diminishing fibrous tissue was observed at the bone/implant interface of Ti-PDA-Cu 0.1 and Ti-PDA-Cu 0.5 groups, in consistency with microCT results. Despite much research being devoted to the interaction between *S. aureus* and osteoblasts, the interplay between *S. aureus* and osteoclasts is much less well explored.[61,62] Hence, this study focused on the direct impact of *S. aureus* on osteoclast activity *in vivo* and elucidated the underlying mechanisms. The results of immunohistochemical and TRAP staining are consistent with the finding from the study by Trouillet *et al.*, who reported that infected mature osteoclasts caused by *S. aureus* upregulated bone resorbing capacity and increased the number of osteoclasts at the site of infection caused by proinflammatory and pro-osteoclastogenic factors resulting from immune responses.[61] Collectively, these results from the animal model of implant-related osteomyelitis clearly demonstrated that Ti-PDA-Cu 0.1 and Ti-PDA-Cu 0.5 groups possess both excellent antibacterial properties and osseointegration capacity in the presence of *S. aureus in vivo*.

In the present study, results from both *in vitro* and *in vivo* studies show that Ti-PDA-Cu 0.1 and Ti-PDA-Cu 0.5 had excellent antibacterial activity, good biocompatibility, as well as enhanced osseointegration performance. Therefore, the present findings support use of Ti-PDA-Cu for prophylaxis of periprosthetic infection such as revision or tumor surgery, which are considered as high infection risk of total joint replacements.[45,63]

5. Conclusion

In conclusion, Cu-deposited Ti substrates have been prepared using PDA-assisted surface modification technology. The antibacterial activity, biocompatibility as well as osseointegration performance of the materials in the presence of bacterial infection were evaluated both *in vitro* and *in vivo*. The functionalized Ti-PDA and Ti-PDA-Cu substrates with different Cu contents exhibited decent biocompatibility to MC3T3-E1 cells. The Ti-PDA-Cu 0.1 and Ti-PDA-Cu 0.5 substrates showed excellent antibacterial activity against both *S. aureus* and *E. coli*. *In vivo* studies based on an animal model of implant-related osteomyelitis revealed that the Ti-PDA-Cu 0.1 and Ti-PDA-Cu 0.5 substrates possessed both excellent antibacterial performance and enhanced osseointegration even in the presence of bacterial infection. Together, findings from this study provide valuable insights toward the design of orthopedic implants which possess both anti-microbial and regenerative properties.

Conflicts of interest

There are no conflicts to declare in this study.

Acknowledgements

This work was supported by the National Natural Science Foundation of China (81471790, 81472060, 31530024, and 81672213), National Key R&D Program of China (2016YFC1100203), Jiangsu Provincial Special Program of Medical Science (BL2012004), Jiangsu Provincial Clinical Orthopedic Center, Key Laboratory of Stem Cells and Biomedical Materials of Jiangsu Province and Chinese Ministry of Science and Technology, and the Priority Academic Program Development (PAPD) of Jiangsu Higher Education Institutions.

References

1 M. Geetha, A. K. Singh, R. Asokamani and A. K. Gogia, *Prog. Mater. Sci.*, 2009, **54**, 397–425.
2 T. Tang and L. Qin, *J. Orthop. Translat.*, 2016, **5**, 69–71.
3 W. J. Metsemakers, K. Kortram, M. Morgenstern, T. F. Moriarty, I. Meex, R. Kuehl, S. Nijs, R. G. Richards, M. Raschke, O. Borens, S. L. Kates, C. Zalavras, P. V. Giannoudis and M. H. Verhofstad, *Injury*, 2017, DOI: 10.1016/j.injury.2017.02.010.
4 R. A. Henderson and M. S. Austin, *J. Arthroplasty*, 2017, **32**, 2056–2059.
5 C. R. Arciola, D. Campoccia, P. Speziale, L. Montanaro and J. W. Costerton, *Biomaterials*, 2012, **33**, 5967–5982.
6 C. R. Arciola, D. Campoccia, G. D. Ehrlich and L. Montanaro, *Adv. Exp. Med. Biol.*, 2015, **830**, 29–46.
7 P. S. Stewart and J. W. Costerton, *Lancet*, 2001, **358**, 135–138.
8 J. A. Inzana, E. M. Schwarz, S. L. Kates and H. A. Awad, *Biomaterials*, 2016, **81**, 58–71.
9 D. P. Lew and F. A. Waldvogel, *Lancet*, 2004, **364**, 369–379.
10 B. H. Kapadia, R. A. Berg, J. A. Daley, J. Fritz, A. Bhave and M. A. Mont, *Lancet*, 2016, **387**, 386–394.
11 R. O. Darouiche, *N. Engl. J. Med.*, 2004, **350**, 1422–1429.
12 A. G. Dalecki, M. Haeili, S. Shah, A. Speer, M. Niederweis, O. Kutsch and F. Wolschendorf, *Antimicrob. Agents Chemother.*, 2015, **59**, 4835–4844.
13 M. E. Villanueva, A. M. Diez, J. A. Gonzalez, C. J. Perez, M. Orrego, L. Piehl, S. Teves and G. J. Copello, *ACS Appl. Mater. Interfaces*, 2016, **8**, 16280–16288.
14 G. Faundez, M. Troncoso, P. Navarrete and G. Figueroa, *BMC Microbiol.*, 2004, **4**, 19.
15 C. Wu, Y. Zhou, M. Xu, P. Han, L. Chen, J. Chang and Y. Xiao, *Biomaterials*, 2013, **34**, 422–433.
16 C. Gerard, L. J. Bordeleau, J. Barralet and C. J. Doillon, *Biomaterials*, 2010, **31**, 824–831.
17 I. Burghardt, F. Luthen, C. Prinz, B. Kreikemeyer, C. Zietz, H. G. Neumann and J. Rychly, *Biomaterials*, 2015, **44**, 36–44.
18 F. Heidenau, W. Mittelmeier, R. Detsch, M. Haenle, F. Stenzel, G. Ziegler and H. Gollwitzer, *J. Mater. Sci.: Mater. Med.*, 2005, **16**, 883–888.
19 D. Sun, D. Xu, C. Yang, J. Chen, M. B. Shahzad, Z. Sun, J. Zhao, T. Gu, K. Yang and G. Wang, *Mater. Sci. Eng., C*, 2016, **69**, 744–750.
20 R. A. Popescu, K. Magyari, A. Vulpoi, D. L. Trandafir, E. Licarete, M. Todea, R. Stefan, C. Voica, D. C. Vodnar,

S. Simon, I. Papuc and L. Baia, *Biomater. Sci.*, 2016, **4**, 1252–1265.
21 J. Liu, F. Li, C. Liu, H. Wang, B. Ren, K. Yang and E. Zhang, *Mater. Sci. Eng., C*, 2014, **35**, 392–400.
22 M. M. Erol, V. Mourino, P. Newby, X. Chatzistavrou, J. A. Roether, L. Hupa and A. R. Boccaccini, *Acta Biomater.*, 2012, **8**, 792–801.
23 Y. Li, L. N. Liu, P. Wan, Z. J. Zhai, Z. Y. Mao, Z. X. Ouyang, D. G. Yu, Q. Sun, L. L. Tan, L. Ren, Z. A. Zhu, Y. Q. Hao, X. H. Qu, K. Yang and K. R. Dai, *Biomaterials*, 2016, **106**, 250–263.
24 B. J. Yoon, F. Xavier, B. R. Walker, S. Grinberg, F. P. Cammisa and C. Abjornson, *Spine J.*, 2016, **16**, 1238–1243.
25 P. J. Rao, M. H. Pelletier, W. R. Walsh and R. J. Mobbs, *Orthop. Surg.*, 2014, **6**, 81–89.
26 N. Harrasser, S. Jussen, A. Obermeir, R. Kmeth, B. Stritzker, H. Gollwitzer and R. Burgkart, *Biomater. Res.*, 2016, **20**, 17.
27 J. Hieda, M. Niinomi, M. Nakai and K. Cho, *Mater. Sci. Eng., C*, 2015, **54**, 1–7.
28 F. Liu, B. Li, J. Y. Sun, H. W. Li, B. Wang and S. L. Zhang, *Appl. Surf. Sci.*, 2012, **258**, 4322–4327.
29 X. Zhao, T. Wang, S. Qian, X. Liu, J. Sun and B. Li, *Int. J. Mol. Sci.*, 2016, **17**, 292.
30 Y. Nie, C. Kalapos, X. Nie, M. Murphy, R. Hussein and J. Zhang, *Ann. Clin. Microbiol. Antimicrob.*, 2010, **9**, 25.
31 H. Ao, Y. Xie, S. Yang, X. Wu, K. Li, X. Zheng and T. Tang, *J. Orthop. Translat.*, 2016, **5**, 16–25.
32 B. Li, J. Chen and J. H. Wang, *J. Biomed. Mater. Res., Part A*, 2006, **79**, 989–998.
33 S. K. Madhurakkat Perikamana, J. Lee, Y. B. Lee, Y. M. Shin, E. J. Lee, A. G. Mikos and H. Shin, *Biomacromolecules*, 2015, **16**, 2541–2555.
34 C. K. Choi, J. Li, K. Wei, Y. J. Xu, L. W. Ho, M. Zhu, K. K. To, C. H. Choi and L. Bian, *J. Am. Chem. Soc.*, 2015, **137**, 7337–7346.
35 H. Lee, J. Rho and P. B. Messersmith, *Adv. Mater.*, 2009, **21**, 431–434.
36 W. B. Tsai, W. T. Chen, H. W. Chien, W. H. Kuo and M. J. Wang, *Acta Biomater.*, 2011, **7**, 4187–4194.
37 D. J. Lee, H. C. Tseng, S. W. Wong, Z. Wang, M. Deng and C. C. Ko, *Bone Res.*, 2015, **3**, 15020.
38 V. Ball, I. Nguyen, M. Haupt, C. Oehr, C. Arnoult, V. Toniazzo and D. Ruch, *J. Colloid Interface Sci.*, 2011, **364**, 359–365.
39 H. Lee, S. M. Dellatore, W. M. Miller and P. B. Messersmith, *Science*, 2007, **318**, 426–430.
40 C. J. Wu, G. X. Zhang, T. Xia, Z. N. Li, K. Zhao, Z. W. Deng, D. Z. Guo and B. Peng, *Mater. Sci. Eng., C*, 2015, **55**, 155–165.
41 J. F. Ou, J. Q. Wang, D. Zhang, P. L. Zhang, S. Liu, P. H. Yan, B. Liu and S. R. Yang, *Colloids Surf., B*, 2010, **76**, 123–127.
42 M. Zhang, X. H. Zhang, X. W. He, L. X. Chen and Y. K. Zhang, *Nanoscale*, 2012, **4**, 3141–3147.
43 H. Cheng, Y. Li, K. F. Huo, B. Gao and W. Xiong, *J. Biomed. Mater. Res., Part A*, 2014, **102**, 3488–3499.
44 Z. He, Q. Zhai, M. Hu, C. Cao, J. Wang, H. Yang and B. Li, *J. Orthop. Translat.*, 2015, **3**, 1–11.
45 S. Thambapillary, R. Dimitriou, K. G. Makridis, E. M. Fragkakis, P. Bobak and P. V. Giannoudis, *J. Arthroplasty*, 2013, **28**, 1381–1385.
46 D. Campoccia, L. Montanaro and C. R. Arciola, *Biomaterials*, 2006, **27**, 2331–2339.
47 A. D. Beswick, K. T. Elvers, A. J. Smith, R. Gooberman-Hill, A. Lovering and A. W. Blom, *BMC Med.*, 2012, **10**, 18.
48 M. Diefenbeck, C. Schrader, F. Gras, T. Muckley, J. Schmidt, S. Zankovych, J. Bossert, K. D. Jandt, A. Volpel, B. W. Sigusch, H. Schubert, S. Bischoff, W. Pfister, B. Edel, M. Faucon and U. Finger, *Biomaterials*, 2016, **101**, 156–164.
49 J. Raphel, M. Holodniy, S. B. Goodman and S. C. Heilshorn, *Biomaterials*, 2016, **84**, 301–314.
50 S. Dong, J. Sun, Y. Li, J. Li, W. Cui and B. Li, *Mater. Sci. Eng., C*, 2014, **35**, 426–433.
51 D. Campoccia, L. Montanaro and C. R. Arciola, *Biomaterials*, 2013, **34**, 8533–8554.
52 S. L. Warnes, V. Caves and C. W. Keevil, *Environ. Microbiol.*, 2012, **14**, 1730–1743.
53 G. Applerot, J. Lellouche, A. Lipovsky, Y. Nitzan, R. Lubart, A. Gedanken and E. Banin, *Small*, 2012, **8**, 3326–3337.
54 W. L. Du, S. S. Niu, Y. L. Xu, Z. R. Xu and C. L. Fan, *Carbohydr. Polym.*, 2009, **75**, 385–389.
55 M. C. Cortizo, M. F. L. de Mele and A. M. Cortizo, *Biol. Trace Elem. Res.*, 2004, **100**, 151–168.
56 E. L. Zhang, L. L. Zheng, J. Liu, B. Bai and C. Liu, *Mater. Sci. Eng., C*, 2015, **46**, 148–157.
57 J. M. O'Connor, M. P. Bonham, E. Turley, A. McKeown, V. J. McKelvey-Martin, W. S. Gilmore and J. J. Strain, *Ann. Nutr. Metab.*, 2003, **47**, 201–206.
58 V. Brinkmann, U. Reichard, C. Goosmann, B. Fauler, Y. Uhlemann, D. S. Weiss, Y. Weinrauch and A. Zychlinsky, *Science*, 2004, **303**, 1532–1535.
59 S. L. Teitelbaum, *Science*, 2000, **289**, 1504–1508.
60 D. Li, K. Gromov, K. Soballe, J. E. Puzas, R. J. O'Keefe, H. Awad, H. Drissi and E. M. Schwarz, *J. Orthop. Res.*, 2008, **26**, 96–105.
61 S. Trouillet-Assant, M. Gallet, P. Nauroy, J. P. Rasigade, S. Flammier, P. Parroche, J. Marvel, T. Ferry, F. Vandenesch, P. Jurdic and F. Laurent, *J. Infect. Dis.*, 2015, **211**, 571–581.
62 C. Dou, C. Zhang, F. Kang, X. Yang, H. Jiang, Y. Bai, J. Xiang, J. Xu and S. Dong, *Biochim. Biophys. Acta*, 2014, **1839**, 1084–1096.
63 J. Voigt, M. Mosier and R. Darouiche, *BMC Infect. Dis.*, 2016, **16**, 749.

